



HAL
open science

Impact study of the wastewater treatment plant effluents on fluorescence of coastal zone water using fluorescence EEM-PARAFAC

Ibrahim El-Nahhal, Roland Redon, Michel Raynaud, Yasser El-Nahhal,
Stéphane Mounier

► To cite this version:

Ibrahim El-Nahhal, Roland Redon, Michel Raynaud, Yasser El-Nahhal, Stéphane Mounier. Impact study of the wastewater treatment plant effluents on fluorescence of coastal zone water using fluorescence EEM-PARAFAC. Environmental Science and Pollution Research, In press, 10.1007/s11356-020-08842-w . hal-02555075

HAL Id: hal-02555075

<https://hal.science/hal-02555075>

Submitted on 27 Apr 2020

HAL is a multi-disciplinary open access archive for the deposit and dissemination of scientific research documents, whether they are published or not. The documents may come from teaching and research institutions in France or abroad, or from public or private research centers.

L'archive ouverte pluridisciplinaire **HAL**, est destinée au dépôt et à la diffusion de documents scientifiques de niveau recherche, publiés ou non, émanant des établissements d'enseignement et de recherche français ou étrangers, des laboratoires publics ou privés.

1
2
3
4
5
6
7
8
9
10 **Impact study of the wastewater treatment plant effluents on fluorescence of coastal zone**
11 **water using fluorescence EEM-PARAFAC.**
12
13
14
15
16

17 EL-Nahhal Ibrahim^{a*}, Redon Roland^a, Raynaud Michel^a, EL-Nahhal Yasser^b, Mounier Stéphane^a
18
19

20 ^a Université de Toulon, Aix Marseille Univ, CNRS, IRD, MIO - CS 60584, 83041 TOULON
21
22 CEDEX 9, France
23
24

25 ^b Department of Environmental and Earth Sciences, Faculty of Science, The Islamic
26
27 University-Gaza Palestinian Territory, P.O Box 108
28
29

30
31 *Corresponding author : elnahhal.i@gmail.com (I.Y.EL-Nahhal)
32
33
34
35
36
37
38
39
40
41
42
43
44
45
46
47
48
49
50
51
52
53
54
55
56
57
58
59
60

61
62
63
64
65 ABSTRACT : Human activity puts pressures on coastal zone altering dissolved organic matter
66
67 quality. No specific self-differentiating fluorescence signal of the anthropogenic DOM in the
68
69 coastal zone is found in the literature. Solar irradiation were conducted on mixed samples of
70
71 River water, sea water, wastewater treatment plant effluent. Excitation Emission Matrices of
72
73 Fluorescence were used to monitor the fate of wastewater treatment plant effluent. Multilinear
74
75 regression of CP/PARAFAC components contribution depending on mixing composition were
76
77 done and was excellent. Kinetics of decreasing contribution versus irradiation time were
78
79 investigated. Second order Kinetics were found for C1 and C2. Distinction between fluorescence
80
81 signal of endmembers was undoable. Wastewater treatment plant endmember after
82
83 photodegradation was highly predominant.
84
85
86
87
88

89
90 Keywords : Fluorescent Organic Matter, EEM-PARAFAC , multilinear regression,
91
92 photodegradation, Coastal zone
93
94
95

96 **1. Introduction**

97
98 Coastal zone is a transitional zone between the terrestrial and oceanic zones (Huguet et al.
99
100 2009) and mixing zone between marine/oceanic waters inputs and the freshwater riverine inputs
101
102 (Parlanti et al. 2000a). Dissolved organic matter (DOM) play an important role in physical,
103
104 chemical functioning of aquatic ecosystems (Hansell 2009) and biogeochemical processes
105
106 (Hansell & Carlson 2014a) and is a heterogenous mixture of organic compounds of both aromatic
107
108 and aliphatic nature (Hansell & Carlson 2014b). Chromophoric Dissolved Organic Matter
109
110 (CDOM) is a fraction of DOM which can interact with light (Coble 1996a; Coble 2007; Lei et al.
111
112 2018) and is ubiquitous in aquatic environmental media (Nelson & Siegel 2013) with a subgroup
113
114
115
116
117
118
119
120

121
122
123 fluorescing FDOM (Coble 1996b; Mostofa et al. 2012). DOM plays a key role in global carbon
124
125 cycle (Hansell 2001) and is highly influenced by continental inputs (Fichot & Benner 2012;
126
127 Yamashita et al. 2013) and by autochthonous sources (Romera-Castillo et al. 2011). Most of
128
129 organic matter in the coastal zone is of terrestrial origin (Hedges et al. 1997; Parlanti et al.
130
131 2000b).
132
133

134
135
136 Human activity has contributed to increased inputs of terrestrial CDOM in aquatic ecosystems
137
138 (Massicotte et al. 2017). Urbanization is increasing and expected to triple between 2000 and 2030
139
140 (Seto et al. 2012) with higher population density and migration to the coastal zone (Hugo 2011a;
141
142 Hugo 2011b). In turn, it changes land cover, hence quality and quantity of DOM in rivers (Seto et
143
144 al. 2012). Anthropogenic sources of organic matter vary from industrial (Carvalho et al. 2008),
145
146 agricultural (Manninen et al. 2018), wastewater treatment plants effluents (Maizel & Remucal
147
148 2017) , landfill leachates (Oloibiri et al. 2017). Moreover, it has been found (Williams et al.
149
150 2016) that anthropogenic influence on urban watersheds caused distinct DOM composition.
151
152 However, contribution of anthropogenic signal of FDOM in coastal zone is not yet well defined
153
154 and evaluated in the literature. Biogeochemistry of natural waters is impacted significantly by
155
156 photo-reactivity of CDOM (Andrew et al. 2013; Lønborg et al. 2016) since photochemistry
157
158 affects bioavailability of DOM (Moran & Zepp 1997; Oleinikova et al. 2017), microbial activity
159
160 (Piccini et al. 2009) and production of DOM of different character (Zhu, Yang, et al. 2017).
161
162
163
164
165
166

167 Partial information can be extracted from global analytical techniques (DOC, TOC, BOD,
168
169 etc...) due to complex composition of DOM. And these techniques are time consuming and
170
171 require elaborated sample preparation. Optical properties of CDOM and FDOM provides a
172
173 valuable tool in delineating DOM sources (Osburn et al. 2016a) and tracking DOM fluxes of
174
175
176
177
178
179
180

181
182
183 terrigenous origin into ocean (Osburn et al. 2016b) enables online or real-time monitoring in
184
185 various media (Helms et al. 2013; Cohen et al. 2014). There are so many advantages of
186
187 fluorescence spectroscopy which is useful, less time-consuming, inexpensive, precise qualitative
188
189 and quantitative technique (Fellman et al. 2010; Zhu et al. 2014) used among varying scientific
190
191 fields (Gao et al. 2017b). Excitation Emission Matrix fluorescence spectroscopy (EEM) has
192
193 furthered scientific research in aquatic systems (Kim & Kim 2015; Dainard et al. 2015; Sgroi et
194
195 al. 2017; Cheng et al. 2018). It enables characterization of optical properties of FDOM due to its
196
197 high sensitivity, good selectivity and non-destruction of samples (Coble 1996c). Coupled with
198
199 Canonical Polyadic / Parallel Factor Analysis (CP/PARAFAC) enables deconvolution of
200
201 overlapping independent EEM spectra into distinct components (Stedmon & Bro 2008a). In
202
203 addition, the use of this technique EEM/PARAFAC in tracing the DOM fractions which is
204
205 cost-effective and rapid in chemistry and aquatic ecology fields is in fact a significant advance in
206
207 those fields (Stedmon et al. 2003a).
208
209
210
211
212
213

214 To the best of our knowledge, there is no previously found pattern or specific
215
216 self-distinguishing fluorescence signal of anthropogenic organic matter in the coastal zone. The
217
218 present study is focussing on wastewater treatment plants effluent discharge in urban river
219
220 systems. Laboratory endmember mixing experiments was conducted of river water , sea water
221
222 and wastewater treatment plant, to define contributions after mixing and solar irradiation
223
224 experiment. The present study is the first of its kind to develop and propose a multivariate linear
225
226 regression for the prediction of FDOM signal and its photodegradation kinetic as a function of
227
228 the mixing composition and solar exposure.
229
230
231
232
233
234
235
236
237
238
239
240

241
242
243
244
245 **2. Material and methods**
246
247
248
249

250 **2.1 Sampling Sites**
251

252 Gapeau river originates at Signes city (43° 17' 24" N, 5° 52' 59" E) and run till the sea at city
253 of Hyères (43°06'42" N, 6°11'33" E) in southeastern part of France (figure 1) with a length of
254 34.4 km (Ollier 1972) and watershed of 544 km² (Ducros et al. 2018) with a pluvial regime.
255 River water (RW) was sampled roughly 500 m before wastewater treatment plant which is
256 located at (43°08'38.6"N 6°05'36.1"E) whereas wastewater treatment plant effluent (WW) was
257 sampled at its output directly. Wastewater treatment plant of La Crau city has a daily volume of
258 0.17 m³/s. Sea water (SW) was sampled at the coastal area of Hyères city at roughly seven meters
259 far from beach (43°06'10.4"N 6°10'38.3"E). Plastic bottle of one liter (cleaned with ethanol
260 100% and three times rinsed with 18.2 MΩ at 25 °C MilliQ water) was used in sampling.
261
262
263
264
265
266
267
268
269
270
271
272
273
274
275
276
277
278
279
280
281
282
283
284
285
286
287
288
289
290
291
292
293
294
295
296
297
298
299
300



Fig. 1. Locations of sampling sites in Southeastern France. RW , WW , SW are the points from left to right colored in red.

361
362
363
364 2.2. Materials of irradiation experiment
365
366

367
368 2.2.1. Filtration
369
370

371 RW , SW , WW samples were filtered using MilliPore filters (Type GNWP 0.20 μm , 47 mm
372 diameter) and filtration kit pre-rinsed with acidified water (10% HNO_3). Filterates were put in a
373 new one liter dark glass bottle (pre-rinsed with 10 % HNO_3 and 3 times with 18.2 $\text{M}\Omega\cdot\text{cm}$ at 25
374 $^\circ\text{C}$ MilliQ-water) and transferred to refrigerator at 4 $^\circ\text{C}$ in the dark. Filtrates were used for
375 preparation of 15 mixtures. The measured pH for RW, WW ,SW were 7.4 ± 0.4 .
376
377
378
379
380
381

382
383 2.2.2. Preparation of mixtures
384
385

386 Fifteen 50 mL quartz vials were washed with reverse osmosis water then transferred to 10 %
387 HNO_3 bath for 24 hours then rinsed three times with 18.2 $\text{M}\Omega\cdot\text{cm}$ at 25 $^\circ\text{C}$ Milli Q-water. Then
388 burnt in oven at 450 $^\circ\text{C}$ for 24 hours to ensure the elimination of organic/inorganic carbon.
389 Fifteen mixtures were fabricated. The exact mixing percentages for each mixture are summarized
390 in table S1 in supplementary information SI. Percentages were taken by weight, assuming a
391 density of 1.00, 1.00 and 1.025 for WW, RW and SW respectively. A serial number was given to
392 the vial according to its corresponding mixture (table S1). Each vial was shaken gently by hand
393 to insure homogeneity of mixtures.
394
395
396
397
398
399
400
401
402
403
404
405
406
407
408
409

410 2.2.3. Irradiation experiments
411
412
413
414
415
416
417
418
419
420

421
422
423 The mixtures were prepared in quartz vials which then were transferred on August 28th 2015
424
425 in the evening to the roof of laboratory MIO/Toulon University (43° 08' 11.2" N 6° 01' 16.7" E).
426
427 These quartz vials were put at sufficient distances to insure receiving same solar irradiation
428
429 conditions. The irradiation started on August 28th 2015 (Day zero) and finished on September
430
431 11th 2015 for a total of ten days of irradiation.
432
433
434
435
436
437

438 2.2.4. Solar irradiation/insolation measurement 439 440 441

442
443 Daily solar insolation data were measured on place in volts using photovoltaic cell (Solar Cell
444
445 9V/109 mA) for each day of irradiation. A mean irradiance of 2 343 volts per day was detected.
446
447 During this period the irradiation is between 5 to 6 kWh.m⁻² corresponding to 39 mW.cm⁻²
448
449 (www.meteofrance.com).
450
451
452

453 2.3. Excitation Emission Matrix EEM fluorescence spectroscopy 454 455 456

457 2.3.1. Irradiated water Sampling 458 459 460 461

462 Three mL aliquots from each 50 mL exposed quartz vial were sampled and transferred into
463
464 10x10 mm quartz cell at different irradiation times. EEMs of solar irradiation experiment sample
465
466 were performed using fluorescence spectrophotometer (F4500, Hitachi). Ultrapure Perkin Elmer
467
468 deionized water was measured to check spectrofluorimeter stability and measure daily the Raman
469
470 peak intensity. Scan speed was set at 2,400 nm.min⁻¹. Emission spectra were collected at 5 nm
471
472
473
474
475
476
477
478
479
480

481
482
483 intervals between 220 and 420 nm, while excitation spectra were measured between 200 and 400
484
485 nm at 5 nm intervals. Slit widths for both excitation and emission wavelengths were set at 5 nm.
486
487
488

489 2.3.2. EEM Data processing

494 2.3.2.1. Raman measurement

496 Water Raman scans of Perkin Elmer blanks were measured for each irradiation day (from Aug.
497
498 28th to Sept. 11th 2015) using the same fluorescence spectrophotometer (F4500, Hitachi). Scans
499 used an excitation wavelength of 350 nm whereas the emission intensities were measured from
500
501 350 nm to 650 nm with a step of 1 nm. Scan speed was 240 nm.mn⁻¹ with the same slit width of
502
503 5 nm on excitation and emission monochromators.
504
505
506

509 2.3.2.2. Raman Normalization

512 Each excitation emission matrix values corresponding to each mixture were normalized to the
513
514 integrated Raman signal measured at the corresponding irradiation date. The integrated Raman
515
516 signal was calculated by integration the area under the curve from 370 nm to 420 nm (Lawaetz &
517
518 Stedmon 2009) and used for EEMs normalisation.
519
520

523 Spectral contribution of each CP/PARAFAC components to total EEM fluorescence was
524
525 determined using CP/PARAFAC algorithm (Bro 1997; Stedmon & Markager 2005a). Finally, the
526
527 150 Raman-corrected EEMs were modelled using a MATLAB software (MathWorks R2015b)
528
529 based on Nway toolbox and DOMFluor toolbox (Stedmon & Bro 2008b). Raman and Rayleigh
530
531 scattering were removed according to Zepp method (Zepp et al. 2004). No inner filter correction
532
533 was done as samples were in linearity domain. Nonnegativity constraints were applied for
534
535
536
537
538
539
540

541 CP/PARAFAC components for excitation and emission loadings. Accepted correct number of
 542 CP/PARAFAC components and model validation was taken according to evaluation of
 543 CONCORDIA score and split-half analysis. No outliers were found in the dataset and a three
 544 components model was validated. Once decomposition is done, for each mixture, contributions of
 545 each components were normalised to the maximum value in the whole EEM dataset, which is, in
 546 that work, the initial one before the start of solar irradiation for all experiments, according to the
 547 following equation :

$$548 C_i^{T_n} = \frac{c_i^{T_n}}{\max(c_i^{T_n})^{\forall n}} \quad (eq.1)$$

549 Where :

550 T_n is the n^{th} day of irradiation. $c_i^{T_n}$ is value of contribution of CP/PARAFAC component i and
 551 $C_i^{T_n}$ the normalised to the maximum contribution of CP/PARAFAC component i from 1 to 3
 552 components.

553 2.4. Multi-linear regression

554 Considering f_{RW} , f_{SW} which are the percentage (w/w) of RW and SW in the quartz vial
 555 mixture respectively, a multi-linear regression was conducted for all f_{RW} , f_{SW} of a fixed
 556 CP/PARAFAC component i for each irradiation day T_n , considering the following general
 557 multilinear regression formula :

$$Y = a_0 + a_1 \cdot X_1 + a_2 \cdot X_2 + \dots + a_n \cdot X_n \quad (\text{eq. 2})$$

2.4.1. Multilinear regression of three endmember

RW, SW and WW mixture is constrained by mass total sum of three content fraction that should be equal to 100 according to the following equation :

$$f_{SW} + f_{RW} + f_{WW} = 100 \quad (0 < f_i < 100) \quad (\text{eq.3})$$

Where f_{SW} , f_{RW} , f_{WW} are content fraction of SW, RW and WW in mass respectively. All percent fractions obviously positive and less than or equal to 100.

Then

$$f_{WW} = 100 - f_{SW} - f_{RW} \quad (\text{eq. 4})$$

By substituting in eq. 2 for f_{WW} where $n=3$, the different terms, the following equation can be obtained :

$$C_i^{Tn} = a_{i,0} + a_{i,1} \cdot f_{SW} + a_{i,2} \cdot f_{RW} + a_{i,3} \cdot f_{WW} \quad (\text{eq.5})$$

Where C_i^{Tn} is normalised contribution of CP/PARAFAC component number i , and $a_{i,1}$, $a_{i,2}$, $a_{i,3}$ the respective partial contribution to this contribution by the three endmember SW, RW and WW. To simplify, C_i^{Tn} is replaced by C_i^* in the next equations

By substituting for f_{WW} by its expression in (eq.4) the following equations can be obtained :

$$C_i^* = a_{i,0} + a_{i,1}f_{SW} + a_{i,2}f_{RW} + a_{i,3} \cdot (100 - f_{SW} - f_{RW}) \quad (\text{eq.6})$$

$$C_i^* = a_{i,0} + a_{i,1}f_{SW} + a_{i,2}f_{RW} + a_{i,3} \cdot 100 - a_{i,3}f_{SW} - a_{i,3}f_{RW} \quad (\text{eq.7})$$

By arranging similar terms together and taking the common factor, the following equation can be obtained :

$$C_i^* = (a_{i,0} + a_{i,3} \cdot 100) + (a_{i,1} - a_{i,3})f_{SW} + (a_{i,2} - a_{i,3})f_{RW} \quad (\text{eq.8})$$

By giving a proper term for the constant and newly modified coefficients to account for f_{WW} term as shown :

$$A_{i,0}^{WW} = (a_{i,0} + a_{i,3} \cdot 100) \quad A_{i,1}^{WW} = (a_{i,1} - a_{i,3}) \quad A_{i,2}^{WW} = (a_{i,2} - a_{i,3})$$

The final multilinear regression equation is obtained as a function of two content fractions of two endmembers :

$$C_i^* = A_{i,0}^{WW} + A_{i,1}^{WW}f_{SW} + A_{i,2}^{WW}f_{RW} \quad (\text{eq.9})$$

721
 722
 723 Where $A^{WW}_{i,0}$, $A^{WW}_{i,1}$ and $A^{WW}_{i,2}$ represent multilinear regression coefficients related to mixing
 724
 725 equation when f_{WW} is expressed in terms of content fraction of the other two endmembers (f_{RW} and
 726
 727 f_{SW}). Any circular permutation can not yield the $a_{i,*}$ coefficients independently.
 728
 729
 730
 731

732 $A^{WW}_{i,0}$ is the constant in the multilinear regression equation which contains information about
 733
 734 WW effect in the multilinear regression, $A^{WW}_{i,1}$ is the coefficient of of content fraction of SW
 735
 736 endmember which not only represent its effect but also the effect of the wastewater treatment
 737
 738 plant effluent WW, $A^{WW}_{i,2}$ is the coefficient of of content fraction of RW endmember which not
 739
 740 only represent its effect but also the effect of WW. Determination of $A^{WW}_{i,0}$, $A^{WW}_{i,1}$ and $A^{WW}_{i,2}$ was
 741
 742 done for each exposition day.
 743
 744
 745
 746
 747
 748

749 2.5. Kinetics

751 The measured irradiation in volts was used as a proxy for photodegradation reaction time . The
 752
 753 determination of the kinetic order of the multilinear regression parameters/coefficients for all T_n
 754
 755 was conducted. These multilinear regression are expressed mathematically as a function of volts :
 756
 757
 758
 759

$$\begin{aligned}
 &A^{WW}_{i,0}(V) \\
 &A^{WW}_{i,1}(V) \\
 &A^{WW}_{i,2}(V)
 \end{aligned}
 \tag{eq.10}$$

760
 761
 762
 763
 764
 765
 766
 767
 768
 769
 770 Where V is received solar irradiation in Volts (V) at each day T_n . CP/PARAFAC contribution
 771
 772 during irradiation experiment can be expressed as a function of content fraction of two
 773
 774 endmember depending on V, which enable kinetic study:
 775
 776
 777
 778
 779
 780

781
782
783
784
785
786
787
788
789
790
791
792
793
794
795
796
797
798
799
800
801
802
803
804
805
806
807
808
809
810
811
812
813
814
815
816
817
818
819
820
821
822
823
824
825
826
827
828
829
830
831
832
833
834
835
836
837
838
839
840

$$C^*_i(V) = A^{WW}_{i,0}(V) + A^{WW}_{i,1}(V) \cdot f_{SW} + A^{WW}_{i,2}(V) \cdot f_{RW} \quad (\text{ep.11})$$

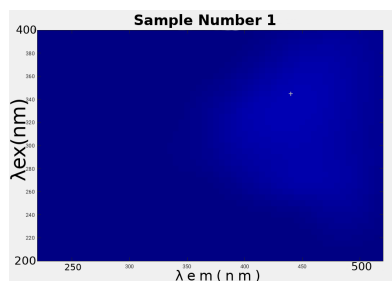
The zeroth, 1st, 2nd and 3rd order kinetics were calculated and compared to find out the most linear model which fits the data (Wright 2004).

3. Results and Discussion

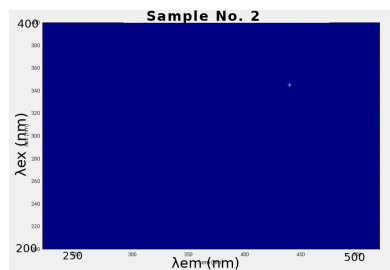
3.1. EEMs Results

Figure 2. shows the excitation emission matrices EEM of fluorescence for the samples numbers 1, 2, 3, 13, 14, 15 which are described in table 2. These EEMs are shown after the removal of Rayleigh and Raman scattering and Raman normalization.

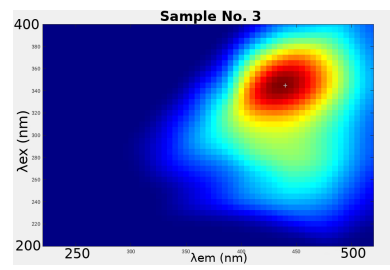
Sample No. :1



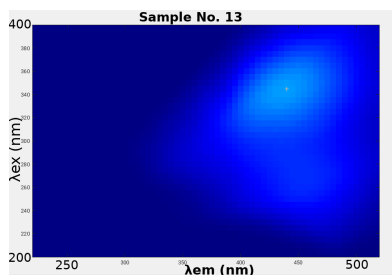
Sample No. : 2



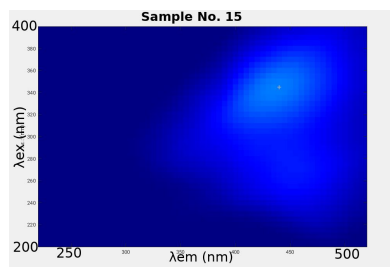
Sample No. : 3



Sample No. : 13



Sample No. : 15



Sample No. : 14

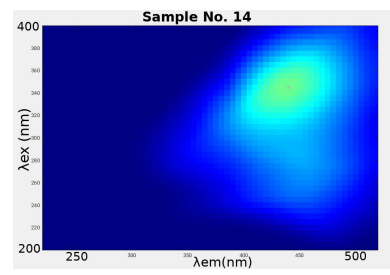
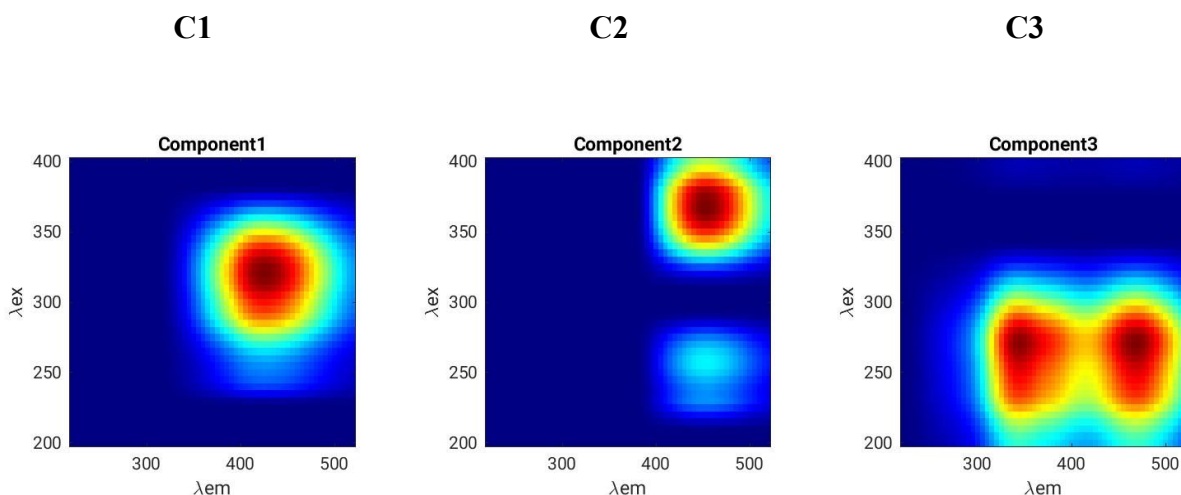


Fig. 2. The excitation emission matrices of Samples number 1 , 2 ,3, 13 , 14 and 15 whose composition is (100,0,0), (0,100,0) ,(0,0,100), (50,0,0), (0,50,0) and (0,0,50) respectively (table S1)

901
902
903 Split-half analysis was conducted for three subsets of the EEM-dataset which asserted the
904 non-existence "finding" of any protein-like fluorescent signal. That's because the CP/PARAFAC
905 algorithm doesn't capture what's already not there.
906
907
908
909
910
911
912
913
914

915 3.2. CP/PARAFAC decomposition results

916
917
918 CORCONDIA analysis showed drop down between four components and five, from near 70 %
919 to less than or around 30 % which surpasses acceptable threshold of 60% where as it showed a
920 value of 80.75 % for three components, indicating that a three-factor model was appropriate. The
921 split-half analysis confirm this three components model. Spectral contour plots of components
922 and their corresponding loadings for both the excitation and the emission wavelengths are shown
923 in figure 3.
924
925
926
927
928
929
930
931
932



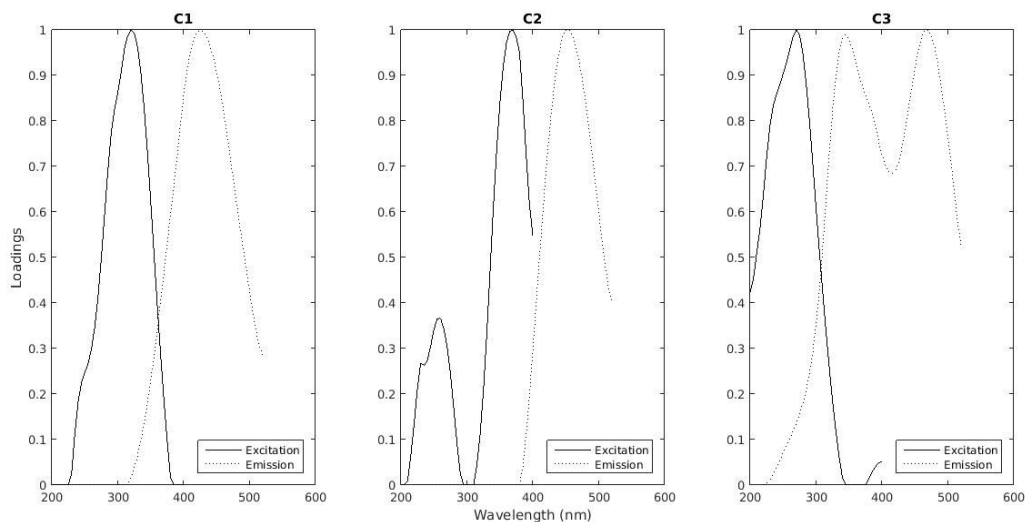


Fig. 3. Contour plots of CP/PARAFAC components found in EEM dataset. Spectral loadings of excitation and emission wavelengths of the three identified CP/PARAFAC in the present study.

Description of excitation and emission pairs of main peak positions for CP/PARAFAC components are summarized in Table 1 and compared to previously identified components and peaks in the literature.

Table 1

Descriptions of CP/PARAFAC components and comparison with literature

Component	$\lambda_{EX}/\lambda_{EM}$ (nm)	Description and references in literature
Component C1	320/425	Component 4 (Stedmon et al. 2003b) : terrestrially derived organic matter
		Peak C (Coble 1996d; Coble et al. 1998) : visible humic-like
		Component 2 (Yamashita et al. 2008a) : terrestrial humic-like
		Component 4 (Yamashita et al. 2008b)
Component C2	370/455	Component 3 (Stedmon et al. 2003c)
		Component G3 (Murphy et al. 2011a)
		Component 3 (Li et al. 2014a)
		Component 7 (Osburn et al. 2016a)
		Component 5 (Bagthoth et al. 2011)
		Component 1 (Zhu et al. 2017a) Humic-Like
Component C3	270/(340) 470	Peak T : Tryptophan like fluorescence (Coble 1996d)
		Q2 (Cory & McKnight 2005)
		Small resemblance to C6 (Zhou et al. 2013) which was Oil-related, degradation product

1081
1082
1083
1084
1085
1086
1087 Based on maximum peak position, these three components have been previously identified
1088 (Table 1). C1, showed an excitation maximum at 320 nm and an emission maximum at 425 nm
1089 and a range of excitation emission wavelengths ($E_x=300-350$ nm, $E_m=400-450$ nm). Previous
1090 studies have associated this component to UVA humic-like fluorescent CP/PARAFAC
1091 component and Peak C (Coble 2007) and peak “ ∞ ” (Parlanti et al. 2000c; Sierra et al. 2005). It
1092 was previously found from terrestrial, anthropogenic, agricultural sources (Stedmon et al. 2003d;
1093 Stedmon & Markager 2005b). C2 component showed an excitation maximum at 370 nm and an
1094 emission maximum at 455 nm and a range of excitation emission wavelengths ($E_x=340-400$ nm,
1095 $E_m= 400-500$ nm). In addition, spectra of C2 resembles spectra of component “G3” which has
1096 $E_{x_{max}}=350$ nm, $E_{m_{max}}=428$ nm in (Murphy et al. 2011b) who have attributed it to wastewater or
1097 nutrient enrichment tracer. This component has also been identified as humic-like component,
1098 similar to “C3” (Li et al. 2014b) which had two excitation maxima (at 250, 350 nm)
1099 corresponding to the same emission maxima (at 440 nm). Furthermore, C2 has very similar
1100 spectra to “C7” from recycled water studies, which included samples of wastewater, treated
1101 water, gray water (Osburn et al. 2016b). C3, showed an excitation maximum at 270 nm and an
1102 emission maximum at 340 nm and 470 nm which is bimodal in emission. It’s range of excitation
1103 emission wavelengths is $E_x=200-300$ nm, $E_m=300-500$ nm. The 1st peak (270/340 nm) is near
1104 the tryptophan-like peak (Coble 1996e). This component could be protein-like component but it
1105 resembles noise.
1106
1107
1108
1109
1110
1111
1112
1113
1114
1115
1116
1117
1118
1119
1120
1121
1122
1123
1124
1125
1126
1127
1128
1129
1130
1131
1132
1133
1134
1135
1136
1137
1138
1139
1140

3.3. Multivariate Linear Regression Parameters

Numerical values of multilinear regression coefficients (eq. 9) for each CP/PARAFAC component C1, C2 and C3 are the following for time zero, i.e. Aug. 28th 2015.

For

$$C1 = 100.45 - 0.99 * f_{SW} - 0.93 * f_{RW} \text{ with coefficient of determination } r^2 \text{ value of } 0.99$$

$$C2 = 98.67 - 0.97 * f_{SW} - 0.92 * f_{RW} \text{ with } r^2 \text{ value of } 0.99$$

$$C3 = 72.84 - 0.66 * f_{SW} - 0.64 * f_{RW} \text{ with } r^2 \text{ value of } 0.84$$

From the above substituted equations, it can be seen that the correlation coefficient is greater than 0.95 for C1 and C2 indicating multilinear regression is excellent. Values of the intercept are always greater than values of coefficients of f_{SW} and f_{RW} by two orders of magnitude. These values of the parameters/coefficients of the multilinear regression are calculated after the Raman unit corrections of the EEM-dataset. Knowing that values of the intercept account for effect of f_{WW} on contribution of CP/PARAFAC component, these results show that contribution of CP/PARAFAC component decreases with increasing f_{SW} or f_{RW} . Indeed, all of coefficients f_{SW} , f_{RW} have negative sign. As a consequence, it can be observed that for $f_{SW}=100$ or $f_{RW}=100$, contributions are weak compared to the $f_{WW}=100$, i.e. $f_{SW}=f_{RW}=0$. These indicated that most of fluorescence contributions are due to WW endmember considering the blank fluorescence $a_{i,0}$ as negligible. Considering that WW is the principal contributor to the all components contribution, there is no specific end member response for SW and RW in these mixtures.

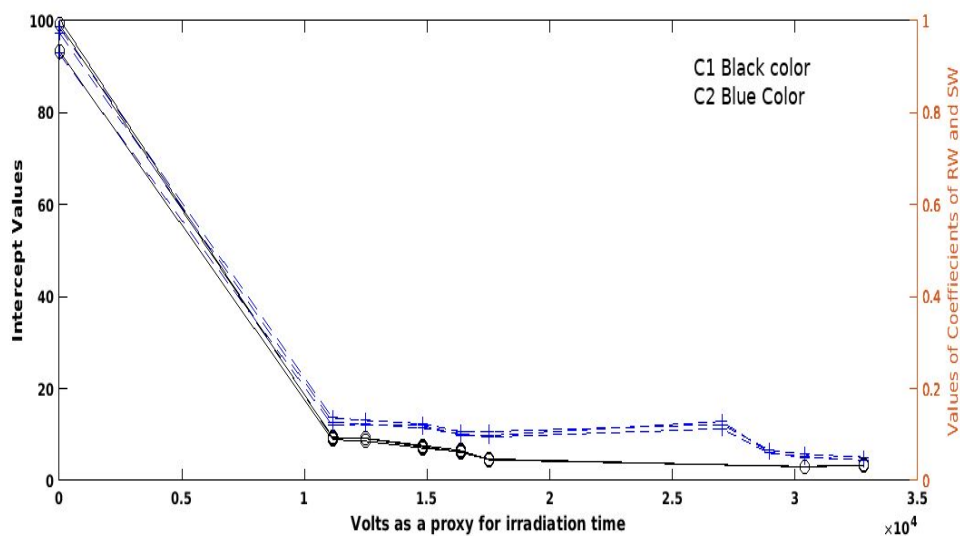


Fig. 4. The variation with irradiation time (volts as proxy for time) of the parameters of multilinear regression (Intercept , absolute values of f_{RW} coefficient, absolute values of f_{SW} coefficient) for C1 and C2 .

The intercept and the coefficients of f_{RW} and f_{SW} of CP/PARAFAC C1 (shown in black) has a faster degradation rate than their counterparts of C2 (shown in blue) as shown in figure 4. which in agreements with the values of the kinetic rate constants as shown in table 6 .

3.4. Determination of kinetic decay coefficient and its kinetic order

The irradiation experiment showed continuous decrease of fluorescence signal with irradiation time. No stable signal or significant fluorescence increase was observed like in other works (; Song et al. 2015; Zhu et al. 2017b). Integrated rate law linear equations of zeroth, 1st, 2nd, and 3rd kinetic order were investigated for each coefficient $A_{i,0}^{WW}$, $A_{i,1}^{WW}$ and $A_{i,3}^{WW}$ to determine kinetics of photodegradation for each multilinear regression parameter. Kinetic order was chosen according to the best coefficient of determination according to kinetic integrated order law,

selecting linear correlation coefficient which must be greater than the threshold 0.75 after eliminating outliers (Wright 2004). Results are presented in table 2 for kinetic order, and kinetic constant are presented in table 3. It was found that all kinetics are 2nd order and are in agreement with a previous work (Yang et al. 2014). Long term photodegradation of fluorescent organic matter is a bimolecular reaction probably involving excited organic matter and organic matter itself. Other work assumed first order kinetic under solar simulated irradiation (Wu et al. 2016) but experiment were done during 12h and under 2.80 mW.cm⁻² (visible) and 70.00 mW.cm⁻², corresponding to the starting point of present irradiation experiment that could be assumed as pseudo-first order kinetic. On the same time, Hee et al 2018 didn't find variation with a 4,2 mW.cm⁻², during 10 hours of exposition.

Table 2

Kinetic order of coefficients of multilinear regression for each CP/PARAFAC with its corresponding r^2 of 2nd order kinetics to the right. "NA" means that correlation coefficient for 2nd order rate was less than 0.75, and was dismissed.

C1						C2						C3		
$A^{ww}_{1,0}$	r^2	$A^{ww}_{1,1}$	r^2	$A^{ww}_{1,2}$	r^2	$A^{ww}_{2,1}$	r^2	$A^{ww}_{2,1}$	r^2	A^{ww}_2	r^2	$A^{ww}_{3,1}$	$A^{ww}_{3,2}$	$A^{ww}_{3,3}$
<i>interpt</i>		(f_{sw})		(f_{rw})		<i>interpt</i>		(f_{sw})		2		<i>interpt</i>	(f_{sw})	(f_{rw})
2	0.94	2	0.95	2	0.96	2	0.83	2	0.78	2	0.82	NA	NA	NA

Table 2 clearly shows that the kinetic order of photodegradation reaction for each parameter of the multi-linear regression for CP/PARAFAC components C1 and C2 are second-order kinetics and the corresponding coefficient of determination r^2 is greater than 0.75 . For the third

CP/PARAFAC component C3 , no order could be found since this component is noise-like component (table 3) and it was neglected from the analysis.

Table 3

Kinetic constant for coefficients of multilinear regression for each CP/PARAFAC component. Values in parenthesis are standard deviation for kinetic constant. All values should be multiplied by 10^6 . NA : Not Available

	C1	C2	C3
$A^{WW}_{*,0}$	9.68(1.00)	4.85(0.78)	NA
<i>interpt</i>			
$A^{WW}_{*,1}$	-987.35(92.31)	-542.80(101.97)	NA
(f_{SW})			
$A^{WW}_{*,2}$	-977.67(83.84)	-552.56(91.70)	NA
(f_{RW})			

Values of kinetic constant for intercept for both C1 and C2 are smaller than those values of kinetic constant for $A^{WW}_{1,1}$ which is coefficient of f_{SW} and $A^{WW}_{1,2}$ which is coefficient of f_{RW} (table 3). This result could be interpreted as follows: C1 and C2 contributions of RW and SW are more sensitive to photodegradation than WW which in turn decays approximately 100 times slower under irradiation suggesting its dominance in the residual fluorescence of both C1 and C2 after long term irradiation. Hence even if there is no specific endmember CP/PARAFAC

1381
1382
1383 contribution, it exist a photosensitivity difference between WW and RW or SW. Under long
1384 irradiation, WW contribution is more resilient and refractory to photodegradation. This difference
1385 of behavior depending on endmember mixing was already observed between terrestrial and
1386 autochthonous organic matter (Zhu et al. 2017c). Small differences were also observed on
1387 reclaimed water using fluorescence matrix regional integration between humic-like and
1388 protein-like under high irradiation (Wu et al. 2016). Therefore, it can be said that wastewater
1389 treatment plant fluorophores are somehow similar to natural fluorophores but more refractory to
1390 photodegradation. Anthropogenic dissolved organic matter, in the present study, remains and
1391 constitute the greatest contribution of CP/PARAFAC components along irradiation process.
1392 Fluorescence signal going to the coastal zone should mainly come from WW endmember.
1393
1394
1395
1396
1397
1398
1399
1400
1401
1402
1403
1404
1405
1406
1407

1408 Comparing C1 versus C2 degradation kinetic, it was observed that humic-like FDOM is more
1409 reactive than protein-like FDOM (Yang et al. 2014). However, results above demonstrated that
1410 it's not so simple. CP/PARAFAC components are constituted by several types of FDOM
1411 fluorophores which behave differently depending on their origin and photosensitivity.
1412
1413
1414
1415
1416
1417
1418

1419 (Timko et al. 2015) found increasing rates of photochemical fluorescent DOM loss with
1420 increasing pH studied thru measurements on the EEMs not between the parameters of multilinear
1421 regression between CP/PARAFAC components and mixing composition . However, *pH* of RW ,
1422 SW and WW were constant ($pH=7.4 \pm 0.4$) in this study suggesting no effect of *pH* in the results
1423 of the kinetic analysis
1424
1425
1426
1427
1428
1429
1430
1431
1432
1433
1434
1435
1436
1437
1438
1439
1440

1441
1442
1443
1444
1445 **4. Conclusions**
1446

1447 In this study, fluorescent conservative behaviour and natural solar changes on three
1448 endmember mixing laboratory experiment were investigated leading to the following conclusions
1449
1450

1451
1452
1453
1454 (1) Multilinear regression model for contribution of CP/PARAFAC components is excellent and
1455 could be done for the three endmembers in addition to being able to study the kinetic evolution.
1456
1457

1458 (2) Two of the three fluorescence CP/PARAFAC extracted component (C1 “terrestrial humic
1459 like” and C2 “humic-like of longer wavelength”) showed a second order photodegradation
1460 toward the irradiation process whatever the endmember mixture composition.
1461
1462

1463 (3) Search for specific self-distinguishing fluorescence signal or signature for river water,
1464 wastewater treatment plants and sea water couldn’t be done in this work, which could be
1465 attributed to the complexity of the anthropogenic and natural dissolved organic matter.
1466
1467

1468 (4) The fluorescence signal of wastewater treatment plant effluent is predominant in the studied
1469 coastal zone, according to the results of photodegradation kinetic constant which favour
1470 anthropogenically-impacted organic matter contribution (100 times less sensitive to
1471 photobleaching). However, its exact contribution couldn’t be found due to inability to calculate
1472 or find its coefficient $a_{i,3}$ in the multilinear regression model independently.
1473
1474

1475 (5) In human impacted coastal zone, residual fluorescent organic matter comes from wastewater
1476 treatment plant effluent, and no specific fluorescence signal either from sea water or from
1477 wastewater treatment plant effluent could be detected near the coast.
1478
1479
1480
1481
1482

1483
1484
1485
1486
1487
1488
1489
1490
1491
1492
1493 **Acknowledgements**
1494
1495
1496
1497
1498
1499
1500

1501
1502
1503
1504
1505 The authors acknowledge Erasmus Mundus/Hermes program for financial support of present
1506
1507 work; Météo-France for providing irradiation data. Christian Martino is thanked for participating
1508
1509 in sampling campaigns. Two anonymous reviewers are thanked for their comments which
1510
1511 ameliorated the quality of this article.
1512

1513
1514
1515
1516 **Declarations of interest** none
1517

1518 **Appendix A. Supplementary Information (SI)**

1519
1520 Supplementary Information to this article can be found in the Supplementary Information (SI)
1521
1522 file
1523
1524

1525 1526 **References**

- 1527
1528
1529
1530 1. Andrew, A.A. et al., 2013. Chromophoric dissolved organic matter (CDOM) in the
1531
1532 Equatorial Atlantic Ocean: Optical properties and their relation to CDOM structure and
1533
1534 source. *Marine chemistry*, 148, pp.33–43. Available at:
1535
1536 <http://dx.doi.org/10.1016/j.marchem.2012.11.001>.
1537
1538
1539 2. Baghoth, S.A., Sharma, S.K. & Amy, G.L., 2011. Tracking natural organic matter (NOM)
1540
1541 in a drinking water treatment plant using fluorescence excitation–emission matrices and
1542
1543 PARAFAC. *Water research*, 45(2), pp.797–809. Available at:
1544
1545 <http://dx.doi.org/10.1016/j.watres.2010.09.005>.
1546
1547
1548 3. Bro, R., 1997. PARAFAC. Tutorial and applications. *Chemometrics and Intelligent*
1549
1550 *Laboratory Systems*, 38(2), pp.149–171. Available at:
1551
1552 [http://dx.doi.org/10.1016/s0169-7439\(97\)00032-4](http://dx.doi.org/10.1016/s0169-7439(97)00032-4).
1553
1554
1555 4. Carvalho, S.I.M. et al., 2008. Effects of solar radiation on the fluorescence properties and
1556
1557
1558
1559
1560

- 1561
1562
1563 molecular weight of fulvic acids from pulp mill effluents. *Chemosphere*, 71(8),
1564 pp.1539–1546. Available at: <http://dx.doi.org/10.1016/j.chemosphere.2007.11.046>.
1565
1566
1567
1568 5. Cheng, C. et al., 2018. Novel insights into variation of dissolved organic matter during
1569 textile wastewater treatment by fluorescence excitation emission matrix. *Chemical*
1570 *engineering journal*, 335, pp.13–21. Available at:
1571 <http://dx.doi.org/10.1016/j.cej.2017.10.059>.
1572
1573
1574
1575
1576 6. Coble, P.G., 1996a. Characterization of marine and terrestrial DOM in seawater using
1577 excitation-emission matrix spectroscopy. *Marine chemistry*, 51(4), pp.325–346. Available
1578 at: [http://dx.doi.org/10.1016/0304-4203\(95\)00062-3](http://dx.doi.org/10.1016/0304-4203(95)00062-3).
1579
1580
1581
1582
1583 7. Coble, P.G., 1996b. Characterization of marine and terrestrial DOM in seawater using
1584 excitation-emission matrix spectroscopy. *Marine chemistry*, 51(4), pp.325–346. Available
1585 at: [http://dx.doi.org/10.1016/0304-4203\(95\)00062-3](http://dx.doi.org/10.1016/0304-4203(95)00062-3).
1586
1587
1588
1589 8. Coble, P.G., 1996c. Characterization of marine and terrestrial DOM in seawater using
1590 excitation-emission matrix spectroscopy. *Marine chemistry*, 51(4), pp.325–346. Available
1591 at: [http://dx.doi.org/10.1016/0304-4203\(95\)00062-3](http://dx.doi.org/10.1016/0304-4203(95)00062-3).
1592
1593
1594
1595 9. Coble, P.G., 1996d. Characterization of marine and terrestrial DOM in seawater using
1596 excitation-emission matrix spectroscopy. *Marine chemistry*, 51(4), pp.325–346. Available
1597 at: [http://dx.doi.org/10.1016/0304-4203\(95\)00062-3](http://dx.doi.org/10.1016/0304-4203(95)00062-3).
1598
1599
1600
1601
1602 10. Coble, P.G., 1996e. Characterization of marine and terrestrial DOM in seawater using
1603 excitation-emission matrix spectroscopy. *Marine chemistry*, 51(4), pp.325–346. Available
1604 at: [http://dx.doi.org/10.1016/0304-4203\(95\)00062-3](http://dx.doi.org/10.1016/0304-4203(95)00062-3).
1605
1606
1607
1608
1609 11. Coble, P.G., 2007. Marine optical biogeochemistry: the chemistry of ocean color.
1610 *Chemical reviews*, 107(2), pp.402–418. Available at:
1611 <http://dx.doi.org/10.1021/cr050350+>.
1612
1613
1614
1615
1616
1617
1618
1619
1620

- 1621
1622
1623
1624
1625
1626
1627
1628
1629
1630
1631
1632
1633
1634
1635
1636
1637
1638
1639
1640
1641
1642
1643
1644
1645
1646
1647
1648
1649
1650
1651
1652
1653
1654
1655
1656
1657
1658
1659
1660
1661
1662
1663
1664
1665
1666
1667
1668
1669
1670
1671
1672
1673
1674
1675
1676
1677
1678
1679
1680
12. Coble, P.G., Del Castillo, C.E. & Avril, B., 1998. Distribution and optical properties of CDOM in the Arabian Sea during the 1995 Southwest Monsoon. *Deep-sea research. Part II, Topical studies in oceanography*, 45(10-11), pp.2195–2223. Available at: [http://dx.doi.org/10.1016/s0967-0645\(98\)00068-x](http://dx.doi.org/10.1016/s0967-0645(98)00068-x).
 13. Cohen, E., Levy, G.J. & Borisover, M., 2014. Fluorescent components of organic matter in wastewater: efficacy and selectivity of the water treatment. *Water research*, 55, pp.323–334. Available at: <http://dx.doi.org/10.1016/j.watres.2014.02.040>.
 14. Cory, R.M. & McKnight, D.M., 2005. Fluorescence Spectroscopy Reveals Ubiquitous Presence of Oxidized and Reduced Quinones in Dissolved Organic Matter. *Environmental science & technology*, 39(21), pp.8142–8149. Available at: <http://dx.doi.org/10.1021/es0506962>.
 15. Dainard, P.G. et al., 2015. Photobleaching of fluorescent dissolved organic matter in Beaufort Sea and North Atlantic Subtropical Gyre. *Marine chemistry*, 177, pp.630–637. Available at: <http://dx.doi.org/10.1016/j.marchem.2015.10.004>.
 16. Ducros, L. et al., 2018. Tritium in river waters from French Mediterranean catchments: Background levels and variability. *The Science of the total environment*, 612, pp.672–682. Available at: <http://dx.doi.org/10.1016/j.scitotenv.2017.08.026>.
 17. Fellman, J.B., Hood, E. & Spencer, R.G.M., 2010. Fluorescence spectroscopy opens new windows into dissolved organic matter dynamics in freshwater ecosystems: A review. *Limnology and oceanography*, 55(6), pp.2452–2462. Available at: <http://dx.doi.org/10.4319/lo.2010.55.6.2452>.
 18. Fichot, C.G. & Benner, R., 2012. The spectral slope coefficient of chromophoric dissolved organic matter (S₂₇₅₋₂₉₅) as a tracer of terrigenous dissolved organic carbon in river-influenced ocean margins. *Limnology and oceanography*, 57(5), pp.1453–1466.

- 1681
1682
1683 Available at: <http://dx.doi.org/10.4319/lo.2012.57.5.1453>.
1684
1685
1686 19. Gao, J. et al., 2017b. Spectral characteristics of dissolved organic matter in various
1687 agricultural soils throughout China. *Chemosphere*, 176, pp.108–116. Available at:
1688 <http://dx.doi.org/10.1016/j.chemosphere.2017.02.104>.
1689
1690
1691
1692 20. Hansell, D., 2001. Marine Dissolved Organic Matter and the Carbon Cycle.
1693 *Oceanography* , 14(4), pp.41–49. Available at:
1694 <http://dx.doi.org/10.5670/oceanog.2001.05>.
1695
1696
1697
1698 21. Hansell, D.A., 2009. Dissolved organic carbon in the carbon cycle of the Indian Ocean. In
1699 *Geophysical Monograph Series*. pp. 217–230. Available at:
1700 <http://dx.doi.org/10.1029/2007gm000684>.
1701
1702
1703
1704 22. Hansell, D.A. & Carlson, C.A., 2014a. *Biogeochemistry of Marine Dissolved Organic*
1705 *Matter*, Academic Press. Available at:
1706 <https://market.android.com/details?id=book-7iKOAwAAQBAJ>.
1707
1708
1709
1710
1711 23. Hansell, D.A. & Carlson, C.A., 2014b. *Biogeochemistry of Marine Dissolved Organic*
1712 *Matter*, Academic Press. Available at:
1713 <https://market.android.com/details?id=book-7iKOAwAAQBAJ>.
1714
1715
1716
1717 24. Hedges, J.I., Keil, R.G. & Benner, R., 1997. What happens to terrestrial organic matter in
1718 the ocean? *Organic geochemistry*, 27(5-6), pp.195–212. Available at:
1719 [http://dx.doi.org/10.1016/s0146-6380\(97\)00066-1](http://dx.doi.org/10.1016/s0146-6380(97)00066-1).
1720
1721
1722
1723
1724 25. Helms, J.R. et al., 2013. Photochemical bleaching of oceanic dissolved organic matter and
1725 its effect on absorption spectral slope and fluorescence. *Marine chemistry*, 155, pp.81–91.
1726 Available at: <http://dx.doi.org/10.1016/j.marchem.2013.05.015>.
1727
1728
1729
1730
1731 26. Hugo, G., 2011a. Future demographic change and its interactions with migration and
1732 climate change. *Global environmental change: human and policy dimensions*, 21,
1733
1734
1735
1736
1737
1738
1739
1740

- 1741
1742
1743 pp.S21–S33. Available at: <http://dx.doi.org/10.1016/j.gloenvcha.2011.09.008>.
1744
1745
1746 27. Hugo, G., 2011b. Future demographic change and its interactions with migration and
1747
1748 climate change. *Global environmental change: human and policy dimensions*, 21,
1749
1750 pp.S21–S33. Available at: <http://dx.doi.org/10.1016/j.gloenvcha.2011.09.008>.
1751
1752 28. Huguet, A. et al., 2009. Properties of fluorescent dissolved organic matter in the Gironde
1753
1754 Estuary. *Organic geochemistry*, 40(6), pp.706–719. Available at:
1755
1756 <http://dx.doi.org/10.1016/j.orggeochem.2009.03.002>.
1757
1758
1759 29. Kim, J. & Kim, G., 2015. Importance of colored dissolved organic matter (CDOM) inputs
1760
1761 from the deep sea to the euphotic zone: Results from the East (Japan) Sea. *Marine*
1762
1763 *chemistry*, 169, pp.33–40. Available at: <http://dx.doi.org/10.1016/j.marchem.2014.12.010>.
1764
1765
1766 30. Lawaetz, A.J. & Stedmon, C.A., 2009. Fluorescence intensity calibration using the
1767
1768 Raman scatter peak of water. *Applied spectroscopy*, 63(8), pp.936–940. Available at:
1769
1770 <http://dx.doi.org/10.1366/000370209788964548>.
1771
1772
1773 31. Lei, X., Pan, J. & Devlin, A.T., 2018. Mixing behavior of chromophoric dissolved
1774
1775 organic matter in the Pearl River Estuary in spring. *Continental shelf research*, 154,
1776
1777 pp.46–54. Available at: <http://dx.doi.org/10.1016/j.csr.2018.01.004>.
1778
1779
1780 32. Li, W.-T. et al., 2014a. Characterization of dissolved organic matter in municipal
1781
1782 wastewater using fluorescence PARAFAC analysis and chromatography
1783
1784 multi-excitation/emission scan: a comparative study. *Environmental science &*
1785
1786 *technology*, 48(5), pp.2603–2609. Available at: <http://dx.doi.org/10.1021/es404624q>.
1787
1788
1789 33. Li, W.-T. et al., 2014b. Characterization of dissolved organic matter in municipal
1790
1791 wastewater using fluorescence PARAFAC analysis and chromatography
1792
1793 multi-excitation/emission scan: a comparative study. *Environmental science &*
1794
1795 *technology*, 48(5), pp.2603–2609. Available at: <http://dx.doi.org/10.1021/es404624q>.
1796
1797
1798
1799
1800

- 1801
1802
1803
1804
1805
1806
1807
1808
1809
1810
1811
1812
1813
1814
1815
1816
1817
1818
1819
1820
1821
1822
1823
1824
1825
1826
1827
1828
1829
1830
1831
1832
1833
1834
1835
1836
1837
1838
1839
1840
1841
1842
1843
1844
1845
1846
1847
1848
1849
1850
1851
1852
1853
1854
1855
1856
1857
1858
1859
1860
34. Lønborg, C. et al., 2016. Photochemical alteration of dissolved organic matter and the subsequent effects on bacterial carbon cycling and diversity. *FEMS microbiology ecology*, 92(5), p.fiw048. Available at: <http://dx.doi.org/10.1093/femsec/fiw048>.
 35. Maizel, A.C. & Remucal, C.K., 2017. The effect of advanced secondary municipal wastewater treatment on the molecular composition of dissolved organic matter. *Water research*, 122, pp.42–52. Available at: <http://dx.doi.org/10.1016/j.watres.2017.05.055>.
 36. Manninen, N. et al., 2018. Effects of agricultural land use on dissolved organic carbon and nitrogen in surface runoff and subsurface drainage. *The Science of the total environment*, 618, pp.1519–1528. Available at: <http://dx.doi.org/10.1016/j.scitotenv.2017.09.319>.
 37. Massicotte, P. et al., 2017. Global distribution of dissolved organic matter along the aquatic continuum: Across rivers, lakes and oceans. *The Science of the total environment*, 609, pp.180–191. Available at: <http://dx.doi.org/10.1016/j.scitotenv.2017.07.076>.
 38. Moran, M.A. & Zepp, R.G., 1997. Role of photoreactions in the formation of biologically labile compounds from dissolved organic matter. *Limnology and oceanography*, 42(6), pp.1307–1316. Available at: <http://dx.doi.org/10.4319/lo.1997.42.6.1307>.
 39. Mostofa, K.M.G. et al., 2012. Fluorescent Dissolved Organic Matter in Natural Waters. In *Environmental Science and Engineering*. pp. 429–559. Available at: http://dx.doi.org/10.1007/978-3-642-32223-5_6.
 40. Murphy, K.R. et al., 2011a. Organic Matter Fluorescence in Municipal Water Recycling Schemes: Toward a Unified PARAFAC Model. *Environmental science & technology*, 45(7), pp.2909–2916. Available at: <http://dx.doi.org/10.1021/es103015e>.
 41. Murphy, K.R. et al., 2011b. Organic Matter Fluorescence in Municipal Water Recycling Schemes: Toward a Unified PARAFAC Model. *Environmental science & technology*,

- 1861
1862
1863 45(7), pp.2909–2916. Available at: <http://dx.doi.org/10.1021/es103015e>.
1864
1865
1866 42. Nelson, N.B. & Siegel, D.A., 2013. The global distribution and dynamics of
1867
1868 chromophoric dissolved organic matter. *Annual review of marine science*, 5, pp.447–476.
1869
1870 Available at: <http://dx.doi.org/10.1146/annurev-marine-120710-100751>.
1871
1872 43. Oleinikova, O.V. et al., 2017. Dissolved organic matter degradation by sunlight
1873
1874 coagulates organo-mineral colloids and produces low-molecular weight fraction of metals
1875
1876 in boreal humic waters. *Geochimica et cosmochimica acta*, 211, pp.97–114. Available at:
1877
1878 <http://dx.doi.org/10.1016/j.gca.2017.05.023>.
1879
1880
1881 44. Ollier, J., 1972. Contribution à l'étude physico-chimique de quelques sources du bassin
1882
1883 versant du Gapeau (Var). *Bulletin mensuel de la Societe linneenne de Lyon*, 41(3),
1884
1885 pp.41–48. Available at: <http://dx.doi.org/10.3406/linly.1972.9979>.
1886
1887
1888 45. Oloibiri, V. et al., 2017. Characterisation of landfill leachate by EEM-PARAFAC-SOM
1889
1890 during physical-chemical treatment by coagulation-flocculation, activated carbon
1891
1892 adsorption and ion exchange. *Chemosphere*, 186, pp.873–883. Available at:
1893
1894 <http://dx.doi.org/10.1016/j.chemosphere.2017.08.035>.
1895
1896
1897 46. Osburn, C.L., Boyd, T.J., et al., 2016a. Optical Proxies for Terrestrial Dissolved Organic
1898
1899 Matter in Estuaries and Coastal Waters. *Frontiers in Marine Science*, 2. Available at:
1900
1901 <http://dx.doi.org/10.3389/fmars.2015.00127>.
1902
1903 47. Osburn, C.L., Boyd, T.J., et al., 2016b. Optical Proxies for Terrestrial Dissolved Organic
1904
1905 Matter in Estuaries and Coastal Waters. *Frontiers in Marine Science*, 2. Available at:
1906
1907 <http://dx.doi.org/10.3389/fmars.2015.00127>.
1908
1909
1910 48. Osburn, C.L., Handsel, L.T., et al., 2016a. Predicting Sources of Dissolved Organic
1911
1912 Nitrogen to an Estuary from an Agro-Urban Coastal Watershed. *Environmental science &*
1913
1914 *technology*, 50(16), pp.8473–8484. Available at:
1915
1916
1917
1918
1919
1920

- 1921
1922
1923
1924 <http://dx.doi.org/10.1021/acs.est.6b00053>.
- 1925
1926 49. Osburn, C.L., Handsel, L.T., et al., 2016b. Predicting Sources of Dissolved Organic
1927
1928 Nitrogen to an Estuary from an Agro-Urban Coastal Watershed. *Environmental science &*
1929
1930 *technology*, 50(16), pp.8473–8484. Available at:
1931
1932 <http://dx.doi.org/10.1021/acs.est.6b00053>.
- 1933
1934 50. Parlanti, E. et al., 2000a. Dissolved organic matter fluorescence spectroscopy as a tool to
1935
1936 estimate biological activity in a coastal zone submitted to anthropogenic inputs. *Organic*
1937
1938 *geochemistry*, 31(12), pp.1765–1781. Available at:
1939
1940 [http://dx.doi.org/10.1016/s0146-6380\(00\)00124-8](http://dx.doi.org/10.1016/s0146-6380(00)00124-8).
- 1941
1942
1943 51. Parlanti, E. et al., 2000b. Dissolved organic matter fluorescence spectroscopy as a tool to
1944
1945 estimate biological activity in a coastal zone submitted to anthropogenic inputs. *Organic*
1946
1947 *geochemistry*, 31(12), pp.1765–1781. Available at:
1948
1949 [http://dx.doi.org/10.1016/s0146-6380\(00\)00124-8](http://dx.doi.org/10.1016/s0146-6380(00)00124-8).
- 1950
1951
1952 52. Parlanti, E. et al., 2000c. Dissolved organic matter fluorescence spectroscopy as a tool to
1953
1954 estimate biological activity in a coastal zone submitted to anthropogenic inputs. *Organic*
1955
1956 *geochemistry*, 31(12), pp.1765–1781. Available at:
1957
1958 [http://dx.doi.org/10.1016/s0146-6380\(00\)00124-8](http://dx.doi.org/10.1016/s0146-6380(00)00124-8).
- 1959
1960
1961 53. Piccini, C. et al., 2009. Alteration of chromophoric dissolved organic matter by solar UV
1962
1963 radiation causes rapid changes in bacterial community composition. *Photochemical &*
1964
1965 *photobiological sciences: Official journal of the European Photochemistry Association*
1966
1967 *and the European Society for Photobiology*, 8(9), pp.1321–1328. Available at:
1968
1969 <http://dx.doi.org/10.1039/b905040j>.
- 1970
1971
1972 54. Romera-Castillo, C. et al., 2011. Net production and consumption of fluorescent colored
1973
1974 dissolved organic matter by natural bacterial assemblages growing on marine
1975
1976
1977
1978
1979
1980

- 1981
1982
1983
1984
1985
1986
1987
1988
1989
1990
1991
1992
1993
1994
1995
1996
1997
1998
1999
2000
2001
2002
2003
2004
2005
2006
2007
2008
2009
2010
2011
2012
2013
2014
2015
2016
2017
2018
2019
2020
2021
2022
2023
2024
2025
2026
2027
2028
2029
2030
2031
2032
2033
2034
2035
2036
2037
2038
2039
2040
- phytoplankton exudates. *Applied and environmental microbiology*, 77(21), pp.7490–7498. Available at: <http://dx.doi.org/10.1128/AEM.00200-11>.
55. Seto, K.C., Güneralp, B. & Hutyra, L.R., 2012. Global forecasts of urban expansion to 2030 and direct impacts on biodiversity and carbon pools. *Proceedings of the National Academy of Sciences of the United States of America*, 109(40), pp.16083–16088. Available at: <http://dx.doi.org/10.1073/pnas.1211658109>.
56. Sgroi, M. et al., 2017. Monitoring the Behavior of Emerging Contaminants in Wastewater-Impacted Rivers Based on the Use of Fluorescence Excitation Emission Matrixes (EEM). *Environmental science & technology*, 51(8), pp.4306–4316. Available at: <http://dx.doi.org/10.1021/acs.est.6b05785>.
57. Sierra, M.M.D. et al., 2005. Fluorescence fingerprint of fulvic and humic acids from varied origins as viewed by single-scan and excitation/emission matrix techniques. *Chemosphere*, 58(6), pp.715–733. Available at: <http://dx.doi.org/10.1016/j.chemosphere.2004.09.038>.
58. Song, W. et al., 2015. Effects of irradiation and pH on fluorescence properties and flocculation of extracellular polymeric substances from the cyanobacterium *Chroococcus minutus*. *Colloids and surfaces. B, Biointerfaces*, 128, pp.115–118. Available at: <http://dx.doi.org/10.1016/j.colsurfb.2015.02.017>.
59. Stedmon, C.A. & Bro, R., 2008a. Characterizing dissolved organic matter fluorescence with parallel factor analysis: a tutorial. *Limnology and oceanography, methods / ASLO*, 6(11), pp.572–579. Available at: <http://dx.doi.org/10.4319/lom.2008.6.572b>.
60. Stedmon, C.A. & Bro, R., 2008b. Characterizing dissolved organic matter fluorescence with parallel factor analysis: a tutorial. *Limnology and oceanography, methods / ASLO*, 6(11), pp.572–579. Available at: <http://dx.doi.org/10.4319/lom.2008.6.572b>.

- 2041
2042
2043
2044
2045
2046
2047
2048
2049
2050
2051
2052
2053
2054
2055
2056
2057
2058
2059
2060
2061
2062
2063
2064
2065
2066
2067
2068
2069
2070
2071
2072
2073
2074
2075
2076
2077
2078
2079
2080
2081
2082
2083
2084
2085
2086
2087
2088
2089
2090
2091
2092
2093
2094
2095
2096
2097
2098
2099
2100
61. Stedmon, C.A. & Markager, S., 2005a. Resolving the variability in dissolved organic matter fluorescence in a temperate estuary and its catchment using PARAFAC analysis. *Limnology and oceanography*, 50(2), pp.686–697. Available at: <http://dx.doi.org/10.4319/lo.2005.50.2.0686>.
62. Stedmon, C.A. & Markager, S., 2005b. Resolving the variability in dissolved organic matter fluorescence in a temperate estuary and its catchment using PARAFAC analysis. *Limnology and oceanography*, 50(2), pp.686–697. Available at: <http://dx.doi.org/10.4319/lo.2005.50.2.0686>.
63. Stedmon, C.A., Markager, S. & Bro, R., 2003a. Tracing dissolved organic matter in aquatic environments using a new approach to fluorescence spectroscopy. *Marine chemistry*, 82(3-4), pp.239–254. Available at: [http://dx.doi.org/10.1016/s0304-4203\(03\)00072-0](http://dx.doi.org/10.1016/s0304-4203(03)00072-0).
64. Stedmon, C.A., Markager, S. & Bro, R., 2003b. Tracing dissolved organic matter in aquatic environments using a new approach to fluorescence spectroscopy. *Marine chemistry*, 82(3-4), pp.239–254. Available at: [http://dx.doi.org/10.1016/s0304-4203\(03\)00072-0](http://dx.doi.org/10.1016/s0304-4203(03)00072-0).
65. Stedmon, C.A., Markager, S. & Bro, R., 2003c. Tracing dissolved organic matter in aquatic environments using a new approach to fluorescence spectroscopy. *Marine chemistry*, 82(3-4), pp.239–254. Available at: [http://dx.doi.org/10.1016/s0304-4203\(03\)00072-0](http://dx.doi.org/10.1016/s0304-4203(03)00072-0).
66. Stedmon, C.A., Markager, S. & Bro, R., 2003d. Tracing dissolved organic matter in aquatic environments using a new approach to fluorescence spectroscopy. *Marine chemistry*, 82(3-4), pp.239–254. Available at: [http://dx.doi.org/10.1016/s0304-4203\(03\)00072-0](http://dx.doi.org/10.1016/s0304-4203(03)00072-0).

- 2101
2102
2103
2104
2105
2106
2107
2108
2109
2110
2111
2112
2113
2114
2115
2116
2117
2118
2119
2120
2121
2122
2123
2124
2125
2126
2127
2128
2129
2130
2131
2132
2133
2134
2135
2136
2137
2138
2139
2140
2141
2142
2143
2144
2145
2146
2147
2148
2149
2150
2151
2152
2153
2154
2155
2156
2157
2158
2159
2160
67. Timko, S.A., Gonsior, M. & Cooper, W.J., 2015. Influence of pH on fluorescent dissolved organic matter photo-degradation. *Water research*, 85, pp.266–274. Available at: <http://dx.doi.org/10.1016/j.watres.2015.08.047>.
68. Williams, C.J. et al., 2016. Human activities cause distinct dissolved organic matter composition across freshwater ecosystems. *Global change biology*, 22(2), pp.613–626. Available at: <http://dx.doi.org/10.1111/gcb.13094>.
69. Wright, M.R., 2004. *Introduction to Chemical Kinetics*, Wiley. Available at: <https://market.android.com/details?id=book-pZQn1RYcFuYC>, 455 pp.
70. Wu, Q. et al., 2016. Removal of fluorescence and ultraviolet absorbance of dissolved organic matter in reclaimed water by solar light. *Journal of environmental sciences*, 43, pp.118–127. Available at: <http://dx.doi.org/10.1016/j.jes.2015.08.021>.
71. Yamashita, Y. et al., 2008a. Assessing the dynamics of dissolved organic matter (DOM) in coastal environments by excitation emission matrix fluorescence and parallel factor analysis (EEM-PARAFAC). *Limnology and oceanography*, 53(5), pp.1900–1908. Available at: <http://dx.doi.org/10.4319/lo.2008.53.5.1900>.
72. Yamashita, Y. et al., 2008b. Assessing the dynamics of dissolved organic matter (DOM) in coastal environments by excitation emission matrix fluorescence and parallel factor analysis (EEM-PARAFAC). *Limnology and oceanography*, 53(5), pp.1900–1908. Available at: <http://dx.doi.org/10.4319/lo.2008.53.5.1900>.
73. Yamashita, Y. et al., 2008c. Assessing the dynamics of dissolved organic matter (DOM) in coastal environments by excitation emission matrix fluorescence and parallel factor analysis (EEM-PARAFAC). *Limnology and oceanography*, 53(5), pp.1900–1908. Available at: <http://dx.doi.org/10.4319/lo.2008.53.5.1900>.
74. Yamashita, Y., Boyer, J.N. & Jaffé, R., 2013. Evaluating the distribution of terrestrial

2161
2162
2163 dissolved organic matter in a complex coastal ecosystem using fluorescence spectroscopy.
2164
2165 *Continental shelf research*, 66, pp.136–144. Available at:
2166
2167 <http://dx.doi.org/10.1016/j.csr.2013.06.010>.

2170 75. Yang, X. et al., 2014. Sunlight-induced changes in chromophores and fluorophores of
2171 wastewater-derived organic matter in receiving waters--the role of salinity. *Water*
2172 *research*, 62, pp.281–292. Available at: <http://dx.doi.org/10.1016/j.watres.2014.05.050>.

2176 76. Zepp, R.G., Sheldon, W.M. & Moran, M.A., 2004. Dissolved organic fluorophores in
2177 southeastern US coastal waters: correction method for eliminating Rayleigh and Raman
2178 scattering peaks in excitation–emission matrices. *Marine chemistry*, 89(1-4), pp.15–36.
2179 Available at: <http://dx.doi.org/10.1016/j.marchem.2004.02.006>.

2185 77. Zhou, Z. et al., 2013. Characterization of oil components from the Deepwater Horizon oil
2186 spill in the Gulf of Mexico using fluorescence EEM and PARAFAC techniques. *Marine*
2187 *chemistry*, 148, pp.10–21. Available at: <http://dx.doi.org/10.1016/j.marchem.2012.10.003>.

2192 78. Zhu, G. et al., 2014. DOM removal by flocculation process: Fluorescence
2193 excitation–emission matrix spectroscopy (EEMs) characterization. *Desalination*, 346,
2194 pp.38–45. Available at: <http://dx.doi.org/10.1016/j.desal.2014.04.031>.

2198 79. Zhu, W.-Z., Yang, G.-P. & Zhang, H.-H., 2017. Photochemical behavior of dissolved and
2199 colloidal organic matter in estuarine and oceanic waters. *The Science of the total*
2200 *environment*, 607-608, pp.214–224. Available at:
2201 <http://dx.doi.org/10.1016/j.scitotenv.2017.06.163>.

2207 80. Zhu, W.-Z., Zhang, J. & Yang, G.-P., 2017a. Mixing behavior and photobleaching of
2208 chromophoric dissolved organic matter in the Changjiang River estuary and the adjacent
2209 East China Sea. *Estuarine, coastal and shelf science*. Available at:
2210 <http://linkinghub.elsevier.com/retrieve/pii/S0272771417302743>.

- 2221
2222
2223
2224
2225
2226
2227
2228
2229
2230
2231
2232
2233
2234
2235
2236
2237
2238
2239
2240
2241
2242
2243
2244
2245
2246
2247
2248
2249
2250
2251
2252
2253
2254
2255
2256
2257
2258
2259
2260
2261
2262
2263
2264
2265
2266
2267
2268
2269
2270
2271
2272
2273
2274
2275
2276
2277
2278
2279
2280
81. Zhu, W.-Z., Zhang, J. & Yang, G.-P., 2017b. Mixing behavior and photobleaching of chromophoric dissolved organic matter in the Changjiang River estuary and the adjacent East China Sea. *Estuarine, coastal and shelf science*. Available at: <http://linkinghub.elsevier.com/retrieve/pii/S0272771417302743>.
82. Zhu, W.-Z., Zhang, J. & Yang, G.-P., 2017c. Mixing behavior and photobleaching of chromophoric dissolved organic matter in the Changjiang River estuary and the adjacent East China Sea. *Estuarine, coastal and shelf science*. Available at: <http://linkinghub.elsevier.com/retrieve/pii/S0272771417302743>.
83. Zhu, W.-Z., Zhang, J., & Yang, G.-P. (2017). Mixing behavior and photobleaching of chromophoric dissolved organic matter in the Changjiang River estuary and the adjacent East China Sea. *Estuarine, Coastal and Shelf Science*. <https://doi.org/10.1016/j.ecss.2017.07.019>

Table S1

Percentages by weight of RW , SW ,WW used in the preparation of fifteen mixtures in Quartz vials for mixing and solar irradiation experiment

	Sample Serial Number														
Endmember	1	2	3	4	5	6	7	8	9	10	11	12	13	14	15
f_{RW}	100	0	0	75	50	25	75	50	25	0	0	0	50	25	25
f_{SW}	0	100	0	25	50	75	0	0	0	25	50	75	25	25	50
f_{WW}	0	0	100	0	0	0	25	50	75	75	50	25	25	50	25